AERO-ACOUSTIC ANALYSIS OF AN AXIAL FAN

Patrice PÉPIN, Marlène SANJOSÉ

École de Technologie Supérieure (ÉTS), Department of Mechanical Engineering, 1100 Notre Dame Street, Montréal, H3C 1K3, Canada

SUMMARY

New fan concepts must achieve high efficiency and low noise levels in order to offer relevant alternatives in an increasingly competitive market. Several research studies show that blade tip clearance has a significant effect on the noise emission and performance of a ducted axial fan. Various numerical analyses are performed on a low-speed USI7[1] axial fan in order to quantify these performance losses associated with the increase in clearance and to evaluate if acoustic models based on steady-state RANS calculations can accurately evaluate the noise emission. The results show that the accuracy of RANS simulations is limited for large tip clearance due to unsteady flow mechanisms. The noise predictions suffer from missing modeling for these complex flow features. Still the aeroacoustic analytical noise models allow to predict the noise increase associated with tip clearance increase.

INTRODUCTION

Industrial fans are critical parts of many processes in the petrochemical, food, textile, mining and other industries. They are also suitable, in smaller sizes, in cooling systems such as computers and electronic systems (such as any high-response controller) and used to supply fresh air or to extract contaminated air [1]. Today, for the health and safety of exposed workers, several limits are imposed on the sound pressure level of noise emissions, as well as on the time of exposure to noise. In Canada, this level is limited to 85 dB(A) in most administrations [2]. This constraint is also important in terms of customer satisfaction. It is therefore crucial to understand the main sources of these noise emissions from fans when designing them, in order to remain competitive in the market.

Several experimental studies show that an increase in blade tip clearance has a significant impact on the noise emissions and performance of an axial fan [3], [4], [5], [6]. Fukano mentions that the blade tip clearance impact is mostly perceived in the broadband noise and that the main cause of

[1] USI7 is a generic low-pressure rotor-only test fan with a low-solidity blade cascade, used by the University of Siegen and others

this increase in sound level is related to a complex vortex structure [6]. It is also something demonstrated by Bharanitharan et *al*. [7] in their comparative numerical simulation study on an axial fan. Their results show that Reynolds-Averaged Navier Stokes (RANS) simulations, which solves the equations for time-averaged flow behaviour, are not sufficient to reproduce the aerodynamic performance of the actual fan. The study presents a percentage error of 19.0 % for a steady-state k-ω Shear-Stress-Transport (k-ω SST) analysis, while the unsteady Reynolds-Averaged Navier Stokes (URANS) k-ω SST model decreases this error to 5.7 % [7]. Corsini et *al*. also mention that RANS simulations are to be favored when the fan is in a stable condition and does not approach a stall zone or when the flow field is not complex [8].

Hence, in order to better visualize and understand these complex flow mechanisms in the tip region, several studies have been carried out using unsteady numerical simulation. Moghadam et *al*. [9] describe a vortex structure that develops at the clearance between the blade tip of an axial fan and its duct using a Large-Eddy Simulation (LES). The results of their analyses were also validated by experimental measurements. The simulations were performed with blade tip clearance ratios of 0.1 %, 0.5 %, and 1 % of the nominal impeller diameter (d_2) [9]. They were able to identify 3 types of vortices whose structure are consistent with past studies [10], [11]. Some of the findings confirm that a larger blade tip clearance (s) increases the diameter and strength of the tip vortex.

The objective of this paper is to evaluate acoustic models based on RANS informed analytical models to evaluate their limitations for use in fan design and optimization procedures. To do this, a numerical study is performed on a low-speed axial fan with two different blade tip clearance sizes.

The first section introduces the studied axial fan and its characteristics. The second section provides an overview of the numerical approached and the different turbulence models. The third section presents a comparison between the aerodynamic performances obtained experimentally and those obtained using RANS calculations. The fourth section present the flow characteristics and their influence on the fan performance. The fifth section presents the results of the analytical acoustic models and the broadband noise contribution.

TEST FAN

The studied configuration is a generic USI7 low-pressure axial fan installed in ducts and experimentally tested at the University of Siegen [12] [13]. The operating condition of the fan will be described at a constant rotation speed in terms of flow rate coefficient φ and pressure rise coefficient ψ. The specific definition of these non-dimensional numbers is provided in Zhu's thesis [13] (see equations (2.1) to (2.5)).

The fan design is detailed in [13]. It is composed of 5 blades, based on NACA 4-digits airfoil sections. The 3D aluminum blades are mounted on an aluminum hub closed with a spherical cap. All fan assembly have a smooth finish. The fan is installed in a circular duct. It has a nominal diameter of 300 mm and a rotational speed (n) of 3000 rpm [13]. The tip clearance which represents the space between the duct and the tip of the blades is characterized by the ratio established between its value and the nominal diameter of the fan (s/d_2). This study used two different tip clearance ratios, 0.1 % and 1 % to evaluate the impacts on aerodynamic and acoustic performance.

NUMERICAL PARAMETERS

In order to capture all the interactions between the system components and the flow, the system is modeled in its entirety for the RANS calculations. The overall numerical configuration of the fan and its system are presented in Figure 1. The computational domain is composed of 3 regions, the *inlet* and *outlet* regions are fixed, while the *rotor* domain is rotating. The purpose of the hemisphere is to mimic the anechoic room in which the assembly is installed. The flow is sucked by the fan, and

the streamlines in the *inlet* region have space to develop naturally before reaching the blades. A mass flow condition is applied over the hemispheric inlet boundary assembly (shown in red in Figure 1) with a direction normal to the local face. All the walls are set with a No-Slip boundary condition except the back wall in contact with the hemisphere, for simplicity. The *rotor* region is defined as a rotating domain where the blades and their hub are selected as fixed within this domain and while the stationary hub and the duct walls are imposed counter-rotating in this domain. In that way, the fan assembly (shown in blue in Figure 1) is rotating. At the outlet, the boundary condition is set with an ambient atmospheric pressure with an allowance of 5 % deviation in average on that surface (shown in green in Figure 1)

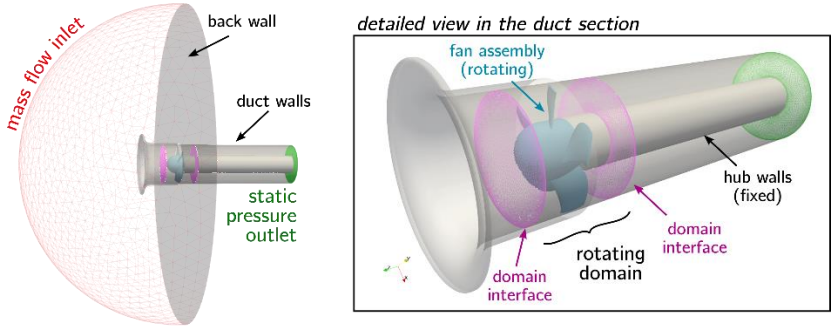

Atmospheric pressure: 1 atm
Air density: 1.16 kg/m^3
Air temperature: 298.15 K
Inlet Turbulence Intensity: 1 %

Figure 1: Computational Domain

The computational grids are generated using the CentaurSoft hybrid mesher. The mesh is composed of triangulated surfaces, prismatic layers to capture the boundary layers and tetrahedral elements in the volume. A transverse plane across the domain and a circular surface at 80 % of the blade span are shown in Figure 2. The same setup is used for both configurations (s/d_2 0.1 % and 1 %). Only the prismatic layers on the duct walls are more constrained with the smaller gap. Two grids have been considered to investigate the convergence, they are identified as *v0* and *v1* in Figure 2. Mesh *v0* consist of 0.45 million elements in the *inlet* region, 0.91 million in the *outlet* region and 6.79 million elements in the *rotor* region for the $s/d_2 = 1\,\%$ configuration. In case of the $s/d_2 = 0.1\,\%$, the number of elements increases up to 0.70 million in the *inlet* region, 0.91 million in the *outlet* region and 7.3 million in the *rotor* region. The second version has approximately 3.5 times this number of elements per zone. The mesh is particularly refined near the duct walls, at the blade tip clearance and on the leading and trailing edges of the different blades. Thus, the number of elements is mainly concentrated in the rotor zone and at the locations with pronounced velocity gradients. The dimensionless mesh size at the wall, y^+, is approximately 4 in average on the blade surfaces with lower values in the tip region.

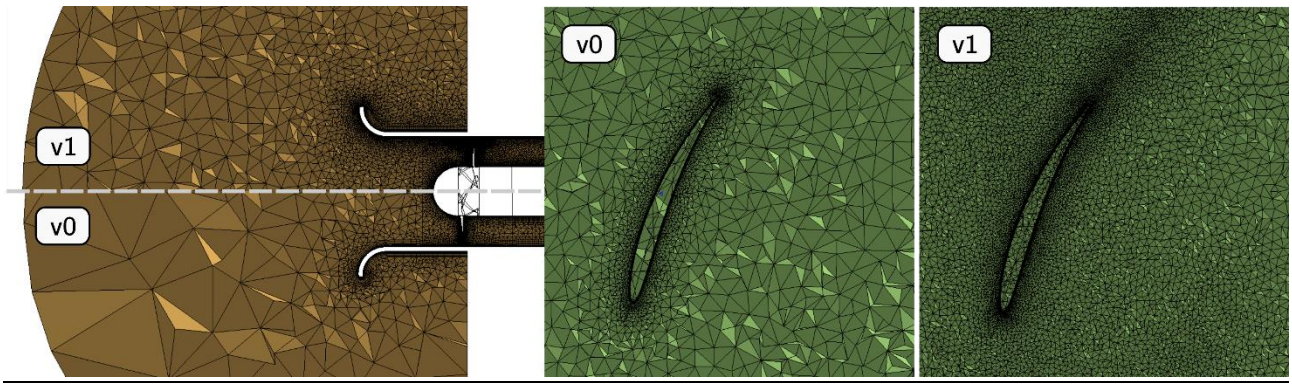

Figure 2: Visualization of the hybrid mesh used in the present study

The numerical simulations are carried out using the Ansys-CFX 19.2 software using RANS modeling. Two different turbulence models are used for the steady state RANS simulations: the k-ω SST because it is a proven model in aerodynamic studies [14] and the Baseline Reynold's

Stress Model (BSL-RSM) because it should provide more accurate turbulence including curvature, pressure-gradient and rotating effects, according to Vlahostergios [15].

A first solution is obtained for the optimal operating point $\varphi = 0.165$ and is used afterwards to initialize the other operating conditions. The convergence checks applied are a maximum iteration criterion of 2000 and an RMS residual convergence criterion of $1.0\text{x}10^{-5}$ on each variable. The values of torques obtained on the 5 blades have converged to a value differing by less than 1 % which confirmed the quality and uniformity of the mesh.

In order to validate the results of these different simulations, the performance values of the fan must be compared with the experimental values. To do so, the total to static pressure rise of the fan is calculated using an area-averaged on two planes in the rotor domain placed at 0.07 m, upstream, and downstream of the middle of the blade. The planes are highlighted in Figure 3.

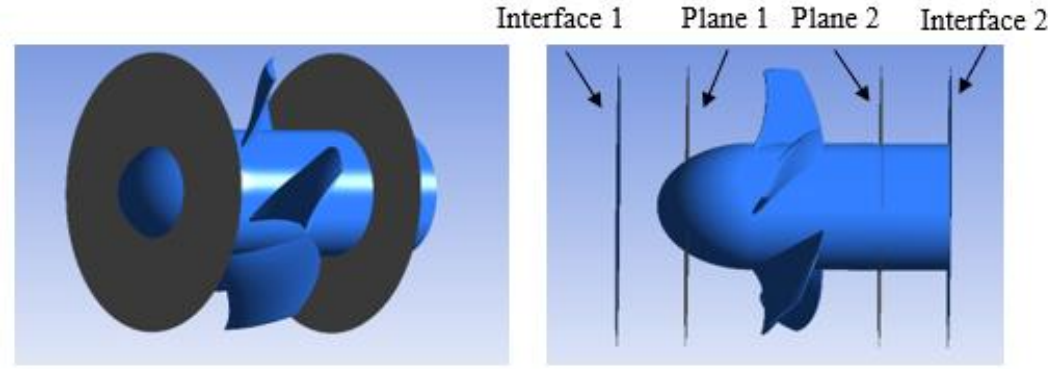

Figure 3 Planes for pressure rise

The calculation of the fan efficiency (see equation (2.3) in Zhu [13]) also requires the computation of the fan torque that accounts for all blades and the rotating hub part (the fan assembly shown in blue in Figure 1). The RANS analyses are then performed on several flow rates for comparison with the experimental performance curve. This is done by changing the mass flow rate imposed at the hemispheric inlet boundary of the domain (in red in Figure 1). The RANS analyses are then performed on several flow rates for comparison with the experimental performance curve and acoustic data provided in [12] [13]. This is done by changing the mass flow rate imposed at the inlet of the fan domain. The variations cover φ from 0.1 to 0.2, the design point is $\varphi = 0.195$ and the optimal point according to experimental campaigns performed at Siegen University [13] is around $\varphi = 0.165$.

The broadband noise emissions are estimated using analytical aeroacoustic models informed by data that are extracted from the RANS simulations [16]. The present study uses the OptiSOUND^{TM} software. The blade is divided into 15 blade strips that are considered as isolated airfoil in translational motion according to Amiet's approach [16], [17]. The far-field acoustic noise spectra of the fan noise emissions is the uncorrelated sum of the far-field acoustic noise spectra of the blade chunks [16]. The aeroacoustic noise mechanisms that are modeled in OptiSOUND^{TM} are the incoming turbulence interaction at the blade leading edge and the trailing-edge noise mechanism (also called self-noise). Both mechanisms at each the airfoil chunks are modeled using the Amiet's aeroacoustic transfer functions [16], [17]. A 2D wavenumber von Kármán spectrum is used to model the incoming turbulence [18], and a Rozenberg wall-pressure spectra together with a Corcos's spanwise coherence length model are used to model the 2D wavenumber wall-pressure spectra [16], [18] [19], [20].

The spectral shape functions are scaled using parameters obtained from the RANS simulations. The required mean flow quantities consist in meridional averaged quantities extracted upstream of the leading-edge and downstream of the trailing-edge. The two cutting lines placed on a meridian plane at about 5 mm from the edges are shown in Figure 4 (left). In addition, boundary layer profiles

extracted at 85 % of the chord (close to the trailing-edge) are extracted to characterize the turbulence that is scattered at the trailing-edge. The locations of extraction are shown in Figure 4 (left).

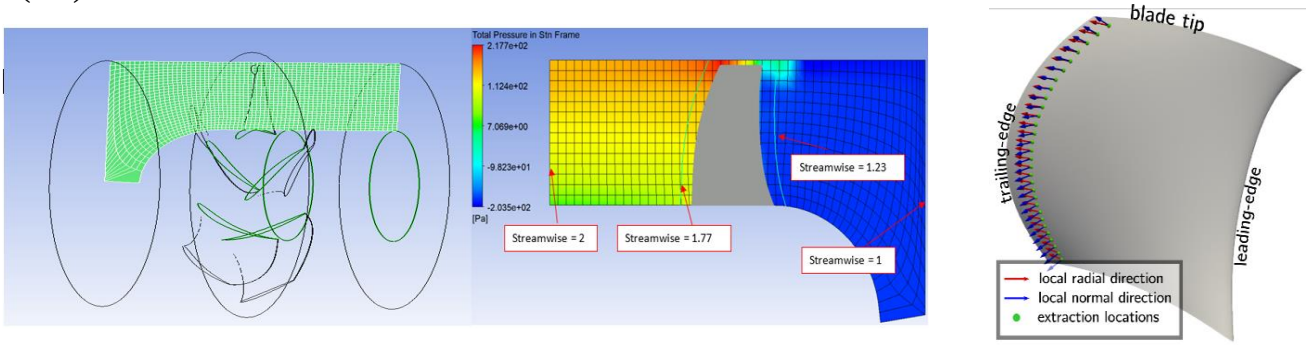

Figure 4: Meridional plan with cutting lines and location of boundary layer extractions

To model the incoming turbulence, in addition to mean velocity components, the turbulence kinetic energy and the turbulent eddy dissipation rate are extracted on the upstream line. These quantities are used to parametrize the von Kármán turbulence spectra at each blade section. Rozenberg's wall-pressure spectra is scaled with the boundary layer thicknesses, the wall shear-stress and the pressure-gradient. In addition, the mean velocity components are extracted on the downstream line, as they are for the aeroacoustic transfer function. The reader is referred to reference [16] for further details, as OptiSOUND^{TM} implements similar approaches.

In order to calculate the acoustic power with OptiSOUND^{TM} a sphere of microphones is defined around the fan center. The radius of the sphere is set to 1 m. The upstream acoustic power will be obtained by integrating over the half upstream part of that observer sphere. Finally, a parametric study is performed to determine the sensitivity of the analysis and the required number of microphones in the observer sphere. A small difference of less than 1 % is observed when more than 30 microphones are placed on the sphere in the meridional plane and 10 in the rotational plane.

AERODYNAMIC PERFORMANCE

In order to evaluate the difference in performance between a tip clearance ratio of 1 % and 0.1 %, the turbulence model k-ω SST is used. Figure 5 includes the refined and coarse mesh, mentioned in the Numerical Parameters section of this study, to see the effect on the fan performance.

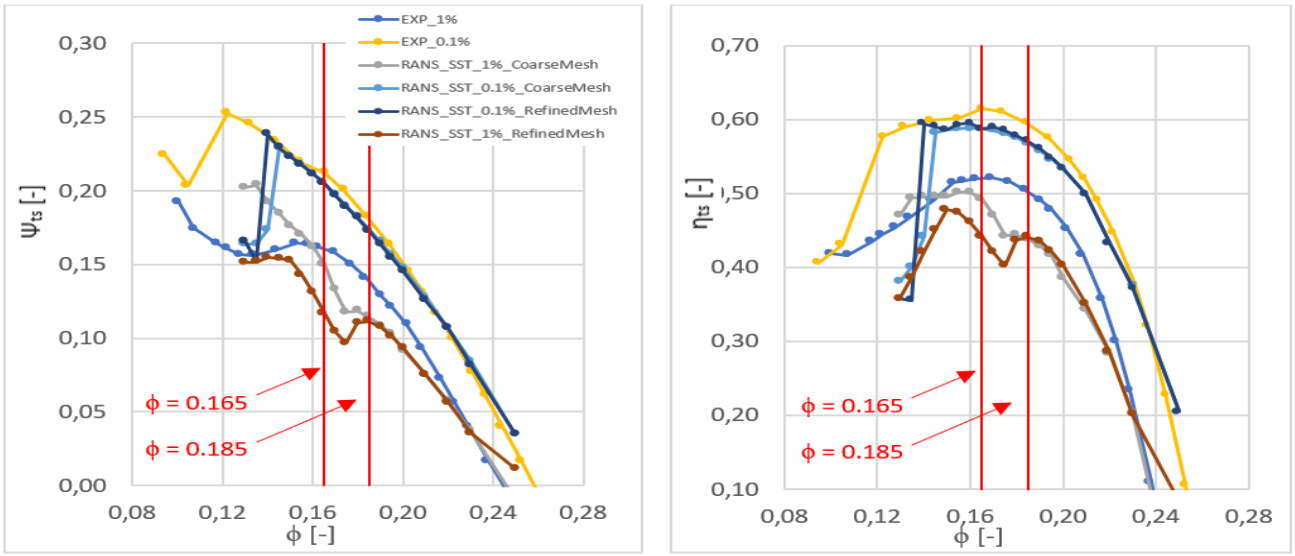

Figure 5: Impact of the tip clearance

As expected, these results show that a larger tip clearance has a major impact on the performance and efficiency of the fan. The difference in the fan efficiency between the two designs can be as much as 35 % in certain operational range. It is also possible to notice that the numerical simulation for the 0.1 % is able to give a very good representation of the actual flow behavior. The only significant error is at very low flow rates, which is most likely that RANS capture stall for a higher flow rate than in the experiments. Hence, it follows Corsini et *al.* [8] conclusion on the fact that RANS calculations should be favored when the fan is in a stable condition and does not approach a stall zone. However, the refined mesh 1 % shows a larger difference, especially in the operational range where a drop in performance occurs compared to the experimental results. While in the experiments the best efficiency point is obtained for $\varphi = 0.165$, this point corresponds to a drop in efficiency in the numerical simulations. Again, this is a limitation of the RANS approach that is not able to capture properly the highly sheared, and vortical tip leakage structure at this specific operating point. The present numerical results for the two blade tip clearances are also consistent with those presented in Tao Zhu's study performed for one blade passage for the same ANSYS-CFX solver using similarly $k-\omega$ SST model [13]. For the refined mesh 0.1 % the performances slightly improve towards the experimental results. Convergence is obtained for this configuration. The mesh refinement does not improve the performance computed for the configuration 1 %. This difference can be explained by the fact that 3D effects are more significant with a larger tip clearance.

The second numerical simulations carried out aim to characterize the differences and effects of the BSL-RSM [15] turbulence model and to determine which one is the most suitable to represent the flow for our study. The results presented below are obtained with the first version of the mesh and with the tip clearance of 1 %.

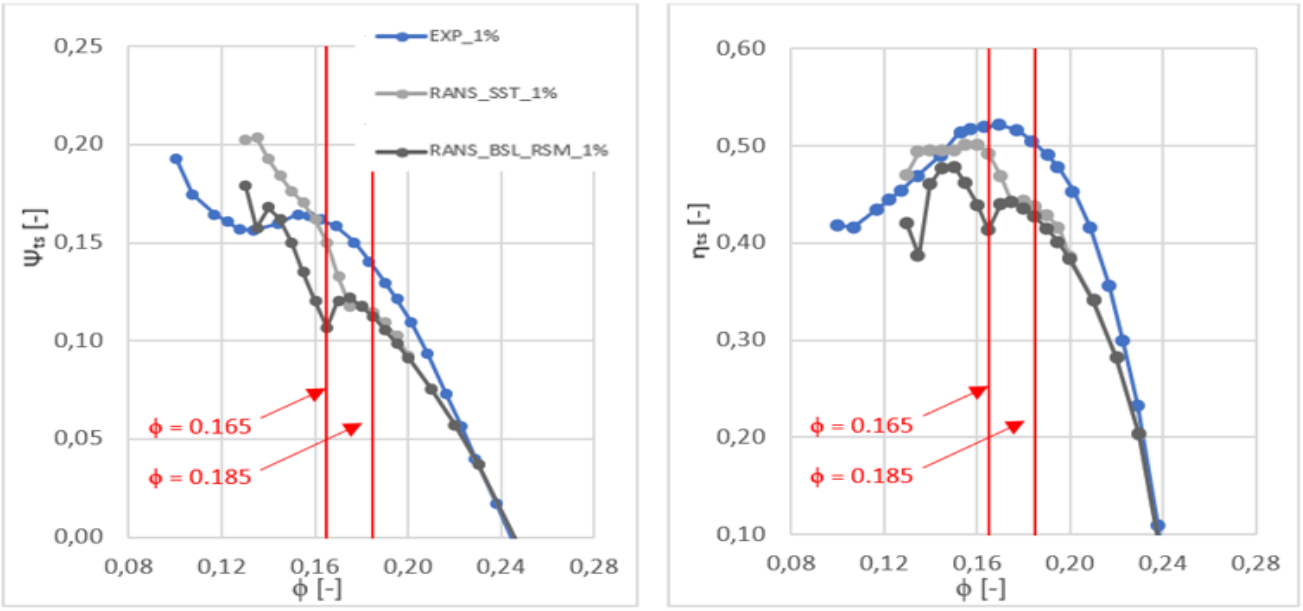

Figure 6: RANS turbulence models comparison

It is possible to notice that the turbulence model k-ω SST shows good results with a percentage error between 1–20 %. However, there is a steep drop in performance compared to the experimental values in the range $\varphi = 0.16 - 0.18$. The calculation in this flow range is not improved in this by the BSL - RSM model neither. It has the highest percentage error ranging between 16 – 37 % and is also not able to give an accurate representation of the flow behavior in the range $\varphi = 0.16 - 0.18$.

The comparison between the numerical simulations and the experimental data for both clearances allowed to validate the calculations and to confirm that the turbulence model k-ω SST is the most accurate RANS calculations for this study, also the results in the range $\varphi = 0.16 - 0.18$ for the 1 % configuration show major discrepancies with the experiments.

FLOW ANALYSES

In order to illustrate the causes in performance drop, the second invariant of velocity gradient tensor (Q-factor) is computed in CFX from the relative velocity. The figure below shows a comparison between the vortex structure generated by a larger tip clearance and flow rates with an isosurface of Q =1.65x10^6 s^{-2} shown in gray.

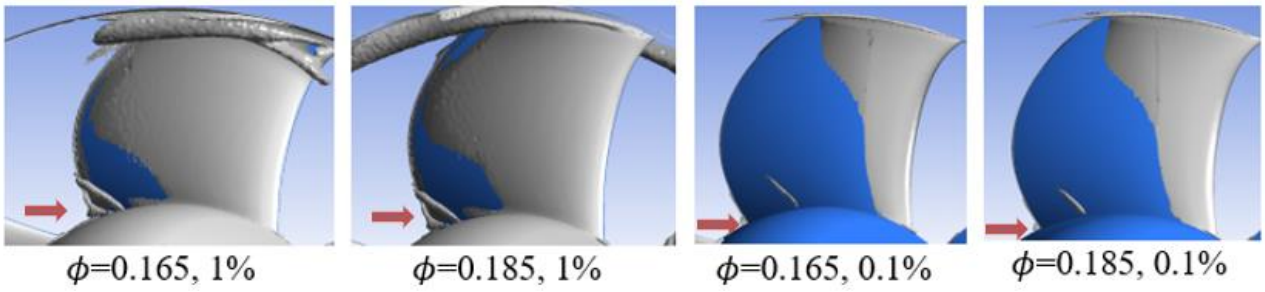

Figure 7: Q factor isosurface comparison

It is possible to notice a significant difference between the vortex structures of the smaller tip clearance. The vortices with the 1 % configuration demonstrate the classical tip leakage vortex at $\varphi = 0.185$. Vortical structures are also present at the leading-edge of the blade tip. The corner recirculation at the hub pointed with red arrows and the tip clearance are much larger on the 1 %. This is the footprint of a change in radial equilibrium of the fan. It can also be observed that the 0.1 % shows small vortex sizes and almost no variation with flow rate increases. The flow is strongly affected by the tip clearance as shown with the performance in Figure 5. The relative flow angle β measured from rotational plane along the upstream and downstream lines, shown in Figure 4 (center), are compared for the two flow coefficients and the two tip clearances in Figure 8. The leading-edge angle profiles show large perturbations induced by the tip clearance. In particular, for $\varphi = 0.165$ the angle increases at the blade foot and a high flow angle is observed at 90 % of the duct section, while it goes to negative value for above locations. This means that reverse flow is observed for that operating point. At the trailing-edge, the profiles are much more consistent between the two clearances for dimensionless radius ranging between 0.6 and 0.85. Around the foot and the tip, the flow is deviated by the flow structures identified in Figure 7.

To estimate the noise sources, as modelled by the aeroacoustic analytical models, the turbulence intensity (I_t) and the turbulence length scale (Λ), made dimensionless with the chord (Λ/c), are shown in Figure 8 (right). Excluding the $\varphi = 0.165$ at 1 % tip clearance simulation, the turbulence intensity at the leading-edge is very low below 1% except in the tip region where it slightly increases up to 2 %. This region is limited to the last extraction point for the simulations with 0.1 % tip gap, while the increase is more progressive (starting a 90 % of dimensionless radius) with the 1 % tip gap. The dimensionless turbulence scale is around 2 % of the chord. The $\varphi = 0.165$ at 1 % tip clearance shows huge increase in the turbulent intensity up to 20 % and turbulence scale. The perturbation occurs on about 50 % of the duct section. It can be concluded that at this particular point the RANS simulation predicts a stalled flow or on the verge of stalling.

The last comparison in Figure 8 (right) shows the momentum thickness of the boundary layers over the blade at the extraction locations shown in Figure 4 (right). The momentum thickness is made dimensionless with the chord length (Θ/c). The ranking between the profiles is here reversed. The higher values (thicker) of momentum thickness are obtained for the configuration with the 0.1 % tip clearance. This is in fact consistent with the higher pressure rise shown for this configuration in Figure 5. Indeed, the blade loading is higher for this configuration, hence the boundary layers experience a higher pressure gradient that tends to thicken the boundary layers.

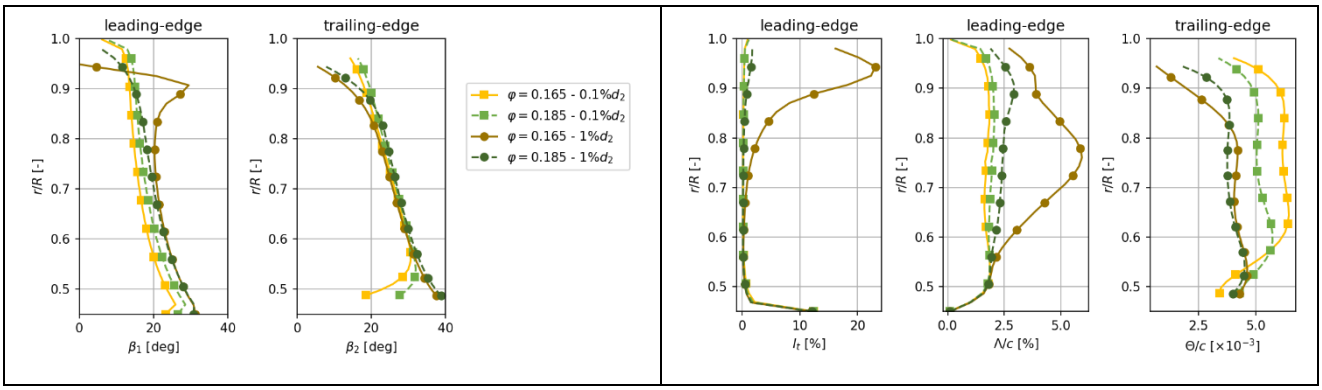

Figure 8: Flow analyses at the leading and trailing edge

These flow analyses identify the different flow features and relate the structures and loading to the overall performances of the fan. The large and intense vortex structures that can be observed with the larger tip clearance are strongly blocking the flow in the tip region. The sudden drop in performance for the large tip clearance is associated with reversed flow, high turbulence intensity and low loading over the last 10 to 20 % of the duct section. This mechanism is probably over-estimated by the RANS simulation that is not able to capture accurately the performance with the 1 % tip clearance (Figure 5).

NUMERICAL ACOUSTIC RESULTS

The acoustic predictions for two mass flow rates using the aeroacoustic analytical models are given in Figure 9. The broad band noise predictions are compared with the upstream acoustic power measured in the anechoic room at Universität Siegen [12]. The reader is referred to the reference [12] for detailed information on measurements and power computation including corrections for the experimental spectra. The leading-edge interaction noise and the trailing-edge turbulence scattering noise are shown with circle and square symbols respectively. Blue shaded lines are associated to the configuration with 1 % tip clearance, while yellow to reddish lines are associated to the 0.1 % clearance. The dashed lines correspond to the sum of the two broadband noise mechanisms. The agreement is only to be discussed at frequencies above 1000 Hz. Indeed, the RANS simulations are not able to capture the unsteady mechanisms responsible for the low frequencies and the sub-harmonics hump that have been investigated in Zhu's thesis [13].

With the lower tip clearance both the high frequency slope and the noise levels are well estimated with the analytical models. The dominant noise mechanism is the trailing-edge noise or self noise of the fan. At higher tip clearance (1 %), the dominant mechanism becomes the leading-edge noise. This is related to the increase in turbulence levels shown in Figure 8. The comparison between the experiments and the predictions is reasonably good in the frequency range above 1000 Hz.

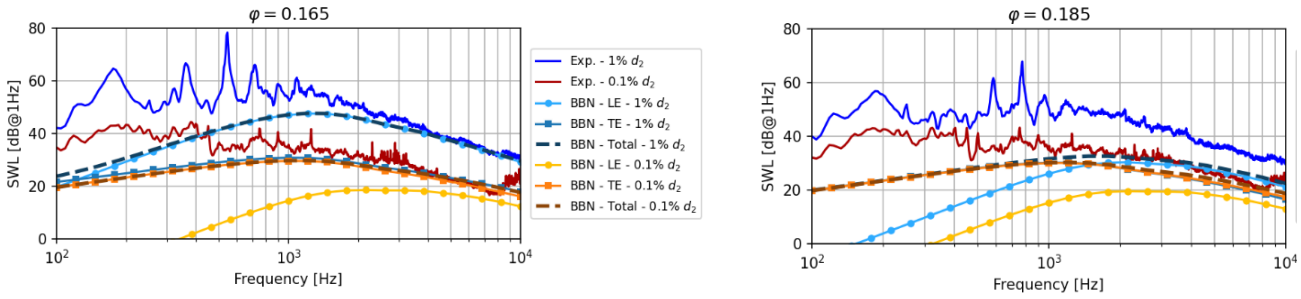

Figure 9: Acoustic results at part load $\varphi = 0.165$ (experimental optimal point) and at near the design point $\varphi = 0.185$

The upstream overall acoustic power is compared between experiments and predictions in Figure 10. The overall power is obtained by integrating the experimental and numerical spectrum

over the range 100 Hz to 10 kHz. It is also possible to identify the leading-edge and the trailing edge mechanism. The experimental sound power levels are 5 to 15 dB above the predictions because of the noise mechanisms (associated to unsteady flow features [13]) that are not accounted for in the RANS simulations. Still the noise level increase caused by the increase in tip clearance is well estimated between 15 to 20 dB, although the range of validity is limited. Again, it is clear that for low tip clearance, the trailing-edge noise mechanism is dominant while the leading edge noise mechanism becomes dominant as the tip clearance is increased.

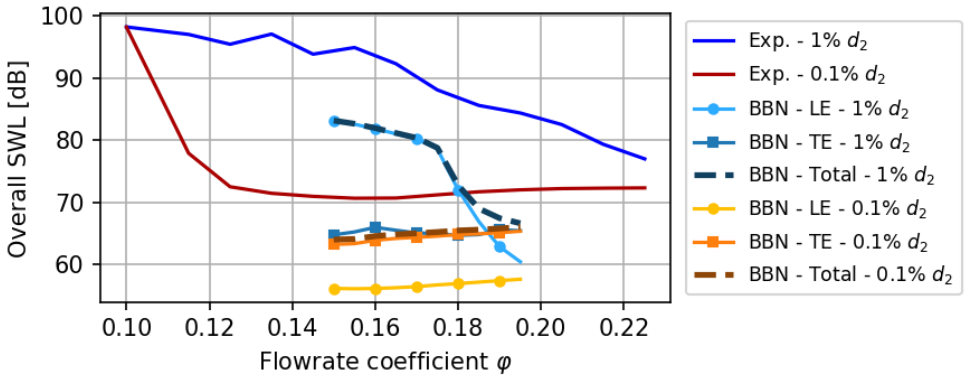

Figure 10: Upstream overall acoustic power as function of mass flow rate.

CONCLUSION

A numerical investigation of the noise mechanisms in a low-speed axial fan has been performed. Several flow rates for constant rotational speed have been computed using ANSYS-CFX RANS solver. Two configurations have been considered with a low (0.1 %) and a high (1 %) tip clearance. Noise emissions are evaluated using aeroacoustic analytical noise models informed from the quantities extracted in the RANS results.

The blade tip clearance has a major impact on the fan performance due to a large vortex structure caused by the tip leakage causing partial stall. The most accurate low-order RANS turbulence model for this flow configuration is the k-ω SST with a percentage error between 1-20 % compared to 16-37 % for the BSL RSM. The sudden drop in performance for higher flow rate than in experiments can be explained by the fact that RANS calculations are not able to capture unsteadiness and the complex tip leakage flow structures for the higher tip clearance configuration. The acoustic power predictions are in good agreements with the measurements for frequencies above 1000 Hz. In particular the analytical models are able to identify the dominant noise sources and provide a good estimation of increase in noise caused by the increase in tip clearance.

An unsteady analysis should be performed at partial load to provide more accurate flow features to improve the noise predictions.

ACKNOWLEDGEMENTS

The authors would like to acknowledge Prof. Thomas Carolus, Dr. Tao Zhu and Ing. Bernd Homrighausen from Universität Siegen for sharing the geometry, operating conditions and detailed measurements on the USI7 configuration. The authors would like to acknowledge Optis Engineering and Dr. Dominic Lallier-Daniels for providing license and support for OptiSOUND™.

BIBLIOGRAPHY

[1] Air Movement and Control Association International, Improving Fan System Performance, 1989.

[2] G. d. Canada, "Limites d'exposition au Bruit au Canada," 23 Octobre 2020. [Online]. Available: https://www.cchst.ca/oshanswers/phys_agents/exposure_can.html.

[3] M. B. Wilkinson and S. J. Van Der Spuy, "The Effect of Fan Tip Configuration On Air-Cooled Condenser Axial Flow Fan Performance," in *Fan 2015*, 2015.

[4] H. Ohashi, "The Effect of Tip Clearance on the Performance of an Axial Flow Fan," Massachusetts Institute of Technology, 1955.

[5] R. Longhouse, "Control of Tip-Vortex Noise of Axial Flow Fans by Rotating Shrouds.," *Journal of Sound and Vibration*, pp. 201-214, 1978.

[6] T. Fukano and C.-M. Jang, "Tip Clearance Noise of Axial Fan Flow Fans Operating at Design and off-Design Condition," *Journal of Sound and Vibration*, pp. 1027-1050, 2004.

[7] K. Bharanitharan, S. Senthilkumar and D. Bhavesh, "Numerical Investigation on Effect of Turbulence Model Selection For Aerodynamic Prediction of Axial Flow Fan," *Research Gate*, pp. 7-8, 2021.

[8] A. Corsini, "A Critical Review of Computational Methods and Their Application in Industrial Fan Design," *Internaltional Scholarly Research Notices*, November 2013.

[9] M. Moghadam Alavi, M. Meinke and W. Schroeder, "Analysis of the acoustic field of a ducted axial fan," in *In 23rd AIAA/CEAS Aeroacoustics Conference*, 2017.

[10] D. You, M. Wang, M. Moin and R. Mittal, "Study of Tip-Clearance flow in Turbomachines Using Large-Eddy Simulation," *Computing in Sciene and Engineering*, 2004.

[11] D. You, M. Wang, M. Moin and R. Mittal, "Vortex Dynamics and Low-Pressure Fluctuations in the Tip-Clearance Flow," *Journal of Fluids Engineering*, pp. 1002-1014, 2007.

[12] T. Zhu and T. Carolus, "Experimental and Unsteady Numerical Investigation of the Tip Clearance Noise of an Axial Fan," in *ASME 2013 Turbine Blade Tip Symposium & Course Week*, Hamburg, Germany, 2013.

[13] T. Zhu, "On the flow Induced Tip Clearance Noise in Axial Fans," Université Siegen, 2016.

[14] F. Menter, "Two-equation eddy-viscosity turbulence models for engineering applications," *AIAA journal, vol. 32, no. 8*, 1994.

[15] Z. Vlahostergios, "Performance Assessment of Reynolds Stress and Eddy Viscosity Models on a Transitional DCA Compressor Blade," *MDPI Aerospace*, p. 13, 13 August 2018.

[16] M. Sanjosé and S. Moreau, "Fast and accurate analytical modeling of broadband noise for a low speed fan," *The Journal of the Acoustical Society of America*, pp. 3103-3113, 2018.

[17] R. K. Amiet, "Noise produced by turbulent flow into a rotor: Theory manual for noise calculation," Technical Report No. CR-181788, 1989.

[18] J. Christophe, "Application of hybrid methods to high frequency aeroacoustics," Ph.D. thesis, von Karman Institute for Fluide Dynamics/ Université Libre de Bruxelles, Brussels, Belgium, 2011.

[19] Y. Rozenberg, "Modélisation analytique du bruit aérodynamique à large bande des machines tournantes: utilisation de calculs moyennés de mécanique des fluides," Ph.D. thesis, Ecole Centrale de Lyon, Lyon, France, 2007.

[20] G. M. Corcos, "Resolution of pressure in turbulence", J. Acoust. Soc. Am. 35(2), 192-199, 1963.